

## Characterization of the mechanical behaviour of Tempcore 500C rebar steel during tensile test necking: experimentation and simulation

Beatriz Hortigon<sup>a,\*</sup>, Fernando Ancio<sup>a</sup>, María A. Herrera-Garrido<sup>a</sup>, José M. Gallardo<sup>b</sup>

<sup>a</sup>Escuela Politécnica Superior, Universidad de Sevilla, Virgen de África 7, 41005 Sevilla, España

<sup>b</sup>Escuela Técnica Superior de Ingeniería, Universidad de Sevilla, Camino de los Descubrimientos s/n, 41092 Sevilla, España

(\*Corresponding author: [bhortigon@us.es](mailto:bhortigon@us.es))

Submitted: 9 November 2020; Accepted: 24 June 2021; Available On-line: 29 September 2021

**ABSTRACT:** The calculation of the true stress and strain values during the tensile test necking phase of smooth ductile metals specimens has been extensively pursued by several authors. A symmetrical neck profile, which leads to axial-symmetrical behaviour, is usually considered. In this study, the neck geometry of Tempcore ribbed bars, the most commonly used steel in reinforced concrete today, is analysed. Knowledge of the true stress and strain values up to failure of this steel is vital since these describe the real behaviour of the steel under extreme conditions. Due to the limited effectiveness of the previously reported theories, an experimental methodology is proposed in order to analyze ribbed bar neck 3D geometry. The results obtained are compared to those of smooth bars of similar steel, both of which are then validated through Finite Element analysis. As a result, the influence of ribbed geometry is found to involve a reduction of true strain values on failure, due to stress concentration occurring in proximity to the root of the transverse ribs affected by necking.

**KEYWORDS:** Failure; Finite element analysis; Necking; Ribbed reinforcement bars; Tempcore steel; Tensile test

**Citation/Citar como:** Hortigon, B.; Ancio, F.; Herrera-Garrido, M.A.; Gallardo, J.M. (2021). "Characterization of the mechanical behaviour of Tempcore 500C rebar steel during tensile test necking: experimentation and simulation". *Rev. Metal.* 57(3): e199. <https://doi.org/10.3989/revmetalm.199>

**RESUMEN:** *Caracterización del comportamiento mecánico durante la fase de estricción de los aceros corrugados Tempcore 500C: experimentación y simulación.* El cálculo de los valores de tensión y deformación verdaderos en probetas cilíndricas de metales dúctiles durante la estricción ha sido ampliamente estudiado por diversos autores partiendo, en todos los casos, de una geometría simétrica del cuello. En este estudio se analiza la evolución del perfil del cuello en las barras corrugadas de los aceros Tempcore, proponiendo una metodología experimental mediante análisis en 3D. Conocer el verdadero comportamiento hasta rotura de este acero es de vital importancia para describir su respuesta ante situaciones límites. Los resultados experimentales obtenidos son comparados con los de barras cilíndricas de acero similar, siendo ambos validados mediante análisis por Elementos Finitos. Dicha comparativa permite comprobar que la existencia de corrugas implica una reducción de la deformación en rotura debido a la concentración de tensiones que se origina en zonas próximas al arranque de las mismas.

**KEYWORDS:** Análisis por elementos finitos; Acero Tempcore; Barras corrugadas de refuerzo; Ensayo de tracción; Estricción; Fractura

**ORCID ID:** Beatriz Hortigon (<https://orcid.org/0000-0002-3362-3648>); Fernando Ancio (<https://orcid.org/0000-0002-2110-0225>); María A. Herrera-Garrido (<https://orcid.org/0000-0002-8660-984X>); José M. Gallardo (<https://orcid.org/0000-0002-7007-2259>)

**Copyright:** © 2021 CSIC. This is an open-access article distributed under the terms of the Creative Commons Attribution 4.0 International (CC BY 4.0) License.

## 1. INTRODUCTION

Understanding the true stress-strain behaviour of ductile materials is extremely important when evaluating mechanical behaviour during welding processes or extreme structural failure loads, as the safety factors of concrete-reinforced bars of a structure submitted to extreme conditions is indispensable to comply with standards. Enhancement of structures ductility, both in terms of design and mechanical behaviour of materials, remains a priority for researchers, manufactureres and governments. According to their engineering strain values at the onset of necking, ribbed reinforcement bars are classified by EN 1992:1-1 (2004).

Ascertaining true stress and strain values on the minimum cross-section is a complex issue due to the state of triaxial stress in the neck. A first approximation based on neck geometry was proposed by Bridgman (1944), from the assumption of axial-symmetrical behaviour, which leads to a symmetrical axial profile, close to an arc of a circle. True stress and strain values are calculated through the equations:

$$\varepsilon_{true} = \ln S_0/S = -2 \ln D/D_0 \quad (1)$$

$$\sigma_{true} = F/S \quad (2)$$

Equivalent stress, defined as that necessary to achieve plasticizing of materials and which is constant throughout the cross sections, is calculated, according to Von Misses yield criterion, through Eq. (3) from true stress values obtained through Eq. (2), depending on the radius of the minimum cross section and the neck-profile curvature radius.

$$\sigma_{equ} = \frac{\sigma_{true}}{(1+2r/a) \ln(1+a/2r)} \quad (3)$$

In order to obviate the need for instantaneous curvature radius measure through the necking process, Bridgman (1944) proposed the following relationship:

$$a/R = \sqrt{\varepsilon_{true} - 0.1} \quad (4)$$

Equation (3) has been subsequently adjusted by Davidenkov and Spiridnova (1946) and Eisenberg and Yen (1983). However, according to Valiente (2000), the best approximation is still given by Bridgman's equation. On the other hand, Eq. (4) has been questioned by several authors (Hang and Rosenfield, 1975; Norris *et al.*, 1978; Le Roy *et al.*, 1981; La Rosa *et al.*, 2003; Celentano *et al.*,

2004; Celentano *et al.*, 2005; Bueno and Villegas, 2011). Norris *et al.* (1978), La Rosa *et al.* (2003), Celentano *et al.* (2004), and Celentano *et al.* (2005) found divergences of between 3 and 10% for the equivalent stress value on fracture. Hanh and Rosenfield (1975), Le Roy *et al.* (1981) and Bueno and Villegas (2011) propose alternative relationships between  $a$  and  $R$ . Finally, concerning the neck profile, the proposal of Chen (1978) and Dong *et al.* (2019) are close to a hyperbola.

Other authors (Mirone, 2004; Ganharul *et al.*, 2012; Donato and Ganharul, 2013) analyse the stress distribution in the neck independently of its profile, and propose an empirical relationship between true and equivalent stress depending solely on instantaneous true strain values. Finally, additional relationships are proposed by Ling (1996) and Mirone *et al.* (2019) in order to obtain true stress values from several parameters such as the strain and stress ones on the onset of necking and the increase in specimen gauge length.

All the experimental techniques used by these authors are mainly based on 2D image analysis and a validation of the results through Finite Element Simulation (FEM). Nowadays, 3D Digital Image Correlation (DIC) is employed to analyse smooth-specimen necking (Kamaya and Kawakubo, 2011; Li *et al.*, 2013; Zhu *et al.*, 2014; Genovese *et al.*, 2016; Rossi *et al.*, 2018). These researchers also found axial-symmetrical behaviour during the necking process.

Nevertheless, the application of all these theories on ribbed bars remains questionable due to their irregular geometry. Paul *et al.* (2014a) and Paul *et al.* (2014b) analyses the high-and-low-cycles fatigue performance of quenched and self-tempered rebar steel manufactured by the Tempcore process using 2D Finite Element Simulation, founding stress accumulation at the root of the transverse ribs. Concerning the 3D simulation of ribbed bars, only Rocha *et al.* (2016) research is available, which concludes that residual stress concentrations are present on the ribbed profile of Tempcore steel bars.

In this work, the mechanical behaviour up to failure of ribbed bars of Tempcore carbon steel is studied with the help of 3D Finite Element Simulation of the necking process. It is shown that a non-symmetrical neck profile develops in correlation with the influence of the ribs on stresses and strains throughout this phenomenon. The results obtained are compared with those of smooth bars of similar steel.

## 2. MATERIALS AND METHODS

The quality (grade) of Tempcore bars tested in this work, provided by the Spanish com-

pany Siderurgica Sevillana S.A., is similar to that of rebar steel 500C, according to European standard EN 1992:1-1 (2004). Both smooth and ribbed specimens, 14 mm in nominal diameter, 8 for each type, have been tested. Chemical composition, as well as the maximum reference values set out in EN 10080 (2005) standard, are shown in Table 1. The geometrical properties of the specimens, as well as the gauge length, can be observed in Fig. 1.

Tensile tests have been carried out accordance with to standards ISO 15630-1 (2010) and ISO 6892-1 (2016). A test speed of  $0.167 \text{ mm s}^{-1}$  was selected for the whole process. Young's modulus was obtained by measuring 3 specimens of each type of steel with a Class 1 extensometer. Axial and transversal displacements have been measured by a high resolution camera synchronized with the test machine.

The evolution of the neck profile has been obtained from 4 specimens of each typology. Twelve images per specimen were captured and processed by means of high-precision image analysis software, resulting in a total of 60 images per each material. As an experimental measure of necking development, the outer diameter profile

was chosen to be recorded on ribbed specimens, as shown in Fig. 2a.

It should be noted that, according to the results obtained from the recordings, there is no axial symmetry on rebar profiles. Therefore, axial-symmetrical behaviour must be rejected and, consequently, a 2D analysis for these bars should also be rejected. Figure 2b shows one instantaneous neck profile shape for one of the tested ribbed bars. Concerning Bridgman's hypothesis (Bridgman, 1944), both right-hand and left-hand profiles present a suitable fit (over 90%) to an arc of a circle. Nevertheless, curvature radius values ( $R_1=84.15 \text{ mm}$ ,  $R_2=72.60 \text{ mm}$ ) and minimum cross section fail to coincide with these two profiles. Due to these results, an experimental methodology by means of a 3D analysis has been carried out in order to obtain more accurate data.

Four tested specimens were joined by drilling a hole in both parts of the fractured specimens that were coincident with the longitudinal axis of the bars (Fig. 3a). Subsequently, a bolt was inserted in order to join these two parts, which had previously been reinforced with adhesive (Figs. 3b and 3c). Finally, the neck area of the joined specimens was scanned using 3D equip-

TABLE 1. Chemical composition (%)

	C	Si	Mn	P	S	Cr	Ni	Mo	Cu	N	Sn	Ti	Co	C <sub>equ</sub>
Smooth	0.15	0.16	0.65	0.027	0.04	0.16	0.10	0.02	0.46	0.009	-	-	-	0.33
Rebar	0.22	0.20	0.71	0.034	0.035	0.17	0.10	0.02	0.46	0.004	0.02	-	-	0.41
EN 1080(*)	0.24			0.055	0.055				0.85			-	-	0.52

(\*)Maximum values

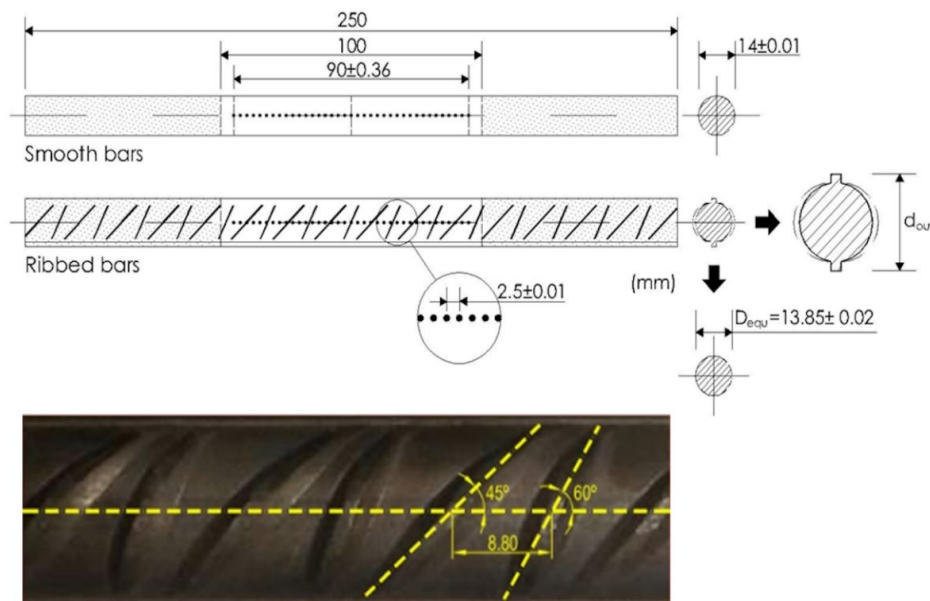


FIGURE 1. Geometry of specimens.

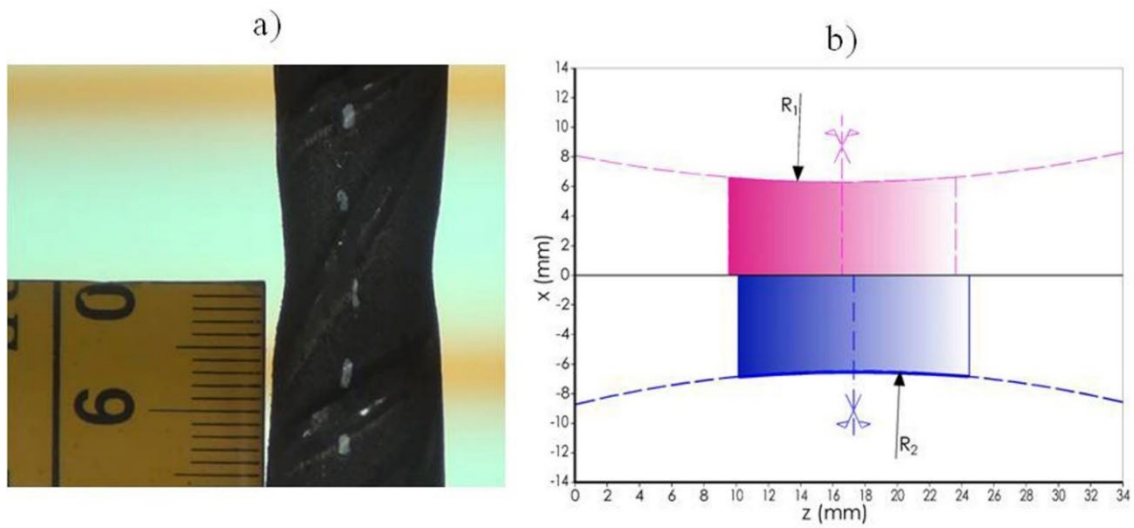


FIGURE 2. a) profile of ribbed bars recorded during the tests, b) neck sample of the profile of ribbed bars.

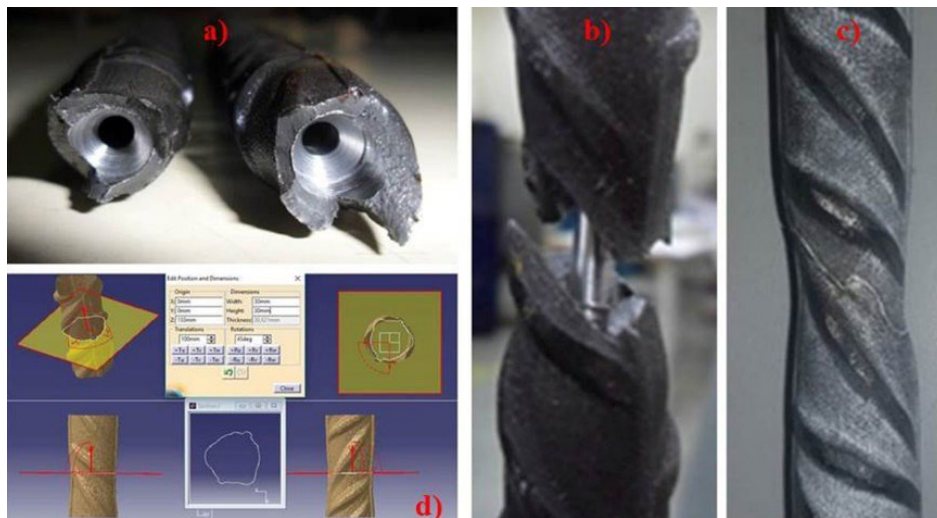


FIGURE 3. Machined joint and scan of ribbed bars.

ment. The cloud of point obtained was processed by means of Catia v5-6, in order to obtain the cross-sections area and the outer diameter data on 19 planes at right angles to the longitudinal axis. (Fig. 3d).

### 3. RESULTS

#### 3.1. Strain-hardening behavior

The engineering stress-strain relationship of smooth and ribbed bars is shown in Fig. 4. Average engineering mechanical values are shown in Table 2. Nomenclature follows the recommendations as per ISO 6892-1 (2016).

True stress and strain values up to the onset of necking have been obtained from Eqs. (5) and (6), proposed by Nadai (1950), which are based

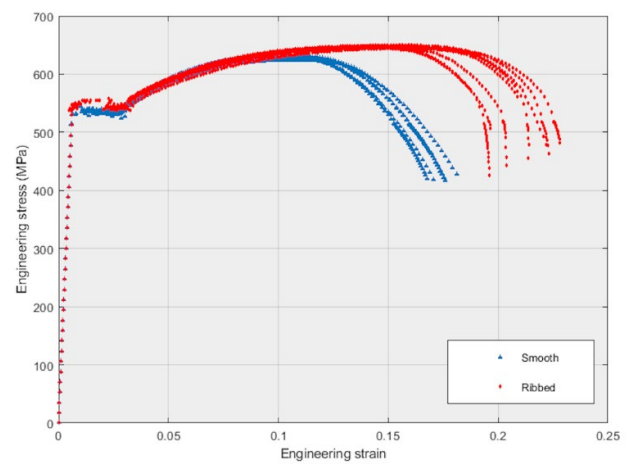


FIGURE 4. Engineering stress-strain relationship for smooth and ribbed bars.

**TABLE 2.** Average engineering mechanical values

	$R_{p,0.2}$ (MPa)	$R_m$ (MPa)	$R_m/R_{p,0.2}$	$A_{gt}$	$A_t$	$E$ (GPa)
Smooth	515.45±11.42	627.65±3.06	1.22±0.03	0.105±0.17	0.174±0.005	195±1.86
Ribbed	521.86±11.13	647.19±1,37	1.24±0.03	0.156±0.008	0.221±0.012	200±2.21

on the material incompressibility and, therefore, cross section reduction is taken into account.

$$\varepsilon_{true} = \ln(1 + A) \quad (5)$$

$$\sigma_{true} = R(1 + A) \quad (6)$$

The average values achieved for true strain on the onset of necking are 0.101 (±0.003) on smooth bars and 0.145 (±0.007) on ribbed bars. Nevertheless, similar mechanical behaviour is observed for both materials through strain hardening phase. According to Hollomon and Jaffe (1945), in the equation  $\sigma_{true} = K\varepsilon_{true}^n$ , shown in Fig. 5, similar values for strain hardening exponent ( $n$ ) are obtained for each of the two materials (Eqs. (7) and (8)), around 0.18, whereby the yield and creep phases are rejected on this fit. Additional information on this issue can be found in Hortigon *et al.* (2017) and Hortigon *et al.* (2019).

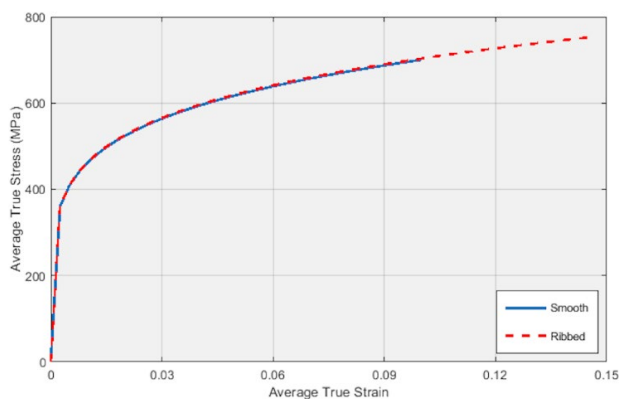
$$\text{Smooth: } \sigma_{true} = 1060.5\varepsilon_{true}^{0.1802} \quad (7)$$

$$\text{Ribbed: } \sigma_{true} = 1065.8\varepsilon_{true}^{0.1806} \quad (8)$$

### 3.2. Necking

In order to obtain equivalent stress values from true strain ones, Eq. (9), as proposed by Mirone (2004), has been used, which is independent of the shape of the neck profile.

$$\sigma_{equ}/\sigma_{true} = 0.9969 - 0.6058(\varepsilon_{true} - \varepsilon_N)^2 + 0.6317(\varepsilon_{true} - \varepsilon_N)^3 - 0.2107(\varepsilon_{true} - \varepsilon_N)^4 \quad (9)$$

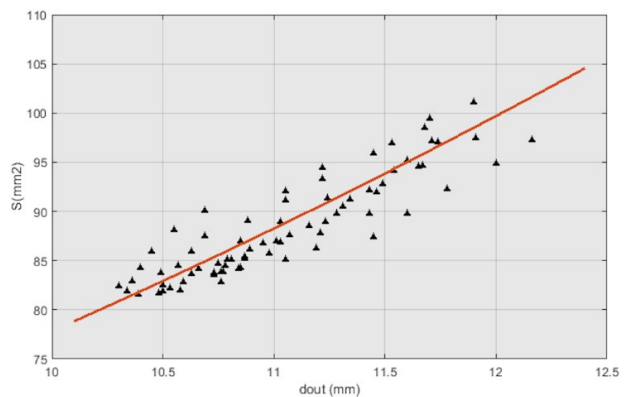

**FIGURE 5.** True stress-strain relationship for smooth and ribbed bars.

Given the symmetrical development of necking in round, smooth bars, minimum values of cross section area have been achieved from minimum diameter measured in the images recorded during the test. Subsequently, true stress and strain values during necking have been calculated through Eqs. (1) and (2).

Regarding ribbed bars, relationship between cross section area and outer diameter (Fig. 6), as obtained from planes at right angles to the longitudinal axis of 3D-scanned neck of bars, shown in Table 3, results in a fit  $R^2=0.9$ :

$$S = 0.4974d_{out}^2 + 28.1334 \quad (10)$$

Despite the fact of a good fit is achieved for Eq. (10), Fig. 7 shows the geometry of some of the cross sections obtained from a specimen, where obvious differences can be observed in the shape of certain sections due to dissimilarities in the ribs strain.


**FIGURE 6.** Neck cross section area vs. measured outer diameter.

Finally, in order to achieve true stress and strain values during the necking,  $F-d_{out}$  data obtained from the recording of the evolution of neck profile during the tests, determined by outer diameter (see Fig. 2), were extrapolated to  $F-S$  data through Eq. (10). Subsequently, true stress and strain values were obtained, from this last relationship, using Eqs. (1) y (2).

The true stress-strain relationship for each type of specimens, including necking data, is compared below. Figure 8 shows results obtained for smooth bars. It should be noted that, taking into account the values of strain hardening

TABLE 3. Outer diameter and cross section area data obtained by means of 3D-scanned images of ribbed bars neck

	$d_{out}$ (mm)	$S$ (mm <sup>2</sup> )		$d_{out}$ (mm)	$S$ (mm <sup>2</sup> )		$d_{out}$ (mm)	$S$ (mm <sup>2</sup> )		$d_{out}$ (mm)	$S$ (mm <sup>2</sup> )
Sp1	11.70	99.44	Sp2	11.74	97.07	Sp3	11.60	95.22	Sp4	11.91	97.46
	11.53	97.01		11.54	94.14		11.49	92.82		11.65	94.58
	11.22	94.45		11.24	91.40		11.31	90.46		11.46	91.97
	11.05	92.07		11.03	88.92		11.16	88.60		11.43	89.81
	10.69	90.16		10.85	86.96		11.03	86.85		11.21	87.79
	10.55	88.10		10.79	85.14		10.87	85.43		10.95	86.81
	10.45	85.98		10.63	83.71		10.78	84.47		10.89	86.14
	10.40	84.31		10.59	82.87		10.76	83.93		10.81	85.14
	10.36	82.98		10.53	82.21		10.73	83.56		10.75	84.71
	<b>10.30(*)</b>	<b>82.41(*)</b>		<b>10.50(*)</b>	<b>81.88(*)</b>		<b>10.49(*)</b>	<b>83.77(*)</b>		<b>10.66(*)</b>	<b>84.18(*)</b>
	10.34	81.86		10.58	82.00		10.57	84.48		10.77	83.92
	10.39	81.56		10.76	82.85		10.63	85.96		10.85	84.26
	10.48	81.67		10.84	84.19		10.69	87.56		11.05	85.17
	10.50	82.57		10.98	85.75		10.88	89.07		11.19	86.28
	10.73	83.80		11.07	87.66		11.05	91.14		11.45	87.45
	10.87	85.26		11.28	89.83		11.22	93.78		11.60	89.80
	11.01	87.01		11.43	92.24		11.45	95.93		11.78	92.25
	11.23	88.97		11.67	94.67		11.68	98.52		12.00	94.89
	11.34	91.27		11.71	97.22		11.90	101.08		12.16	97.30

(\*)Minimum cross section

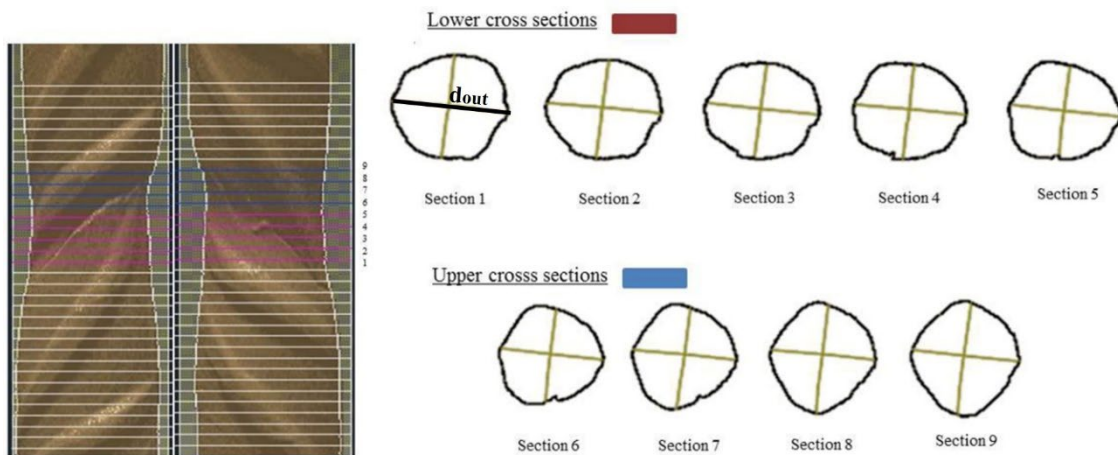


FIGURE 7. Sample of cross section of ribbed bar neck obtained from 3D scanned images.

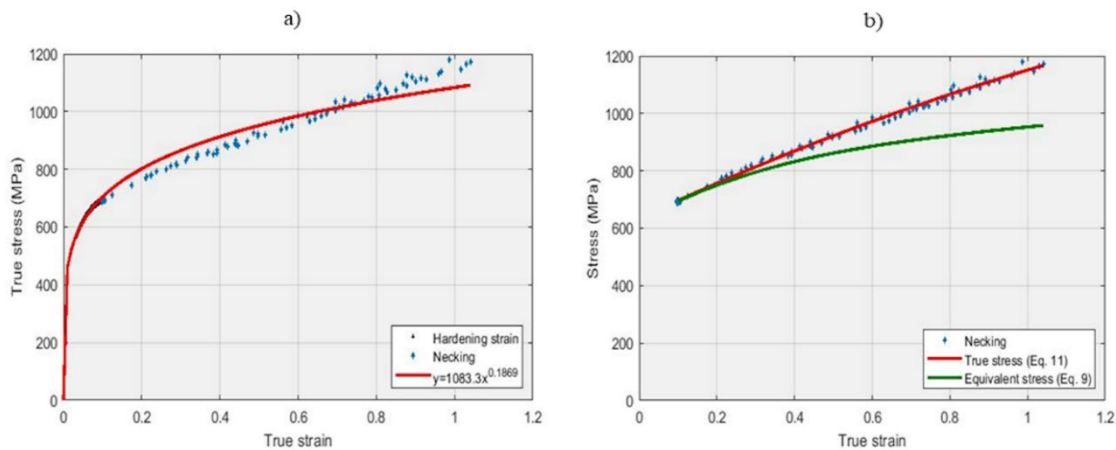


FIGURE 8. True stress-strain relationship up to failure for round smooth bars. Adjustment to: a) the Hollomon equation, b) polynomial equation (+ equivalent stress).

phase, fitting to Hollomon’s equation (Hollomon and Jaffe, 1945) (Fig. 8a), as used by several authors (La Rosa *et al.*, 2003; Celentano *et al.*, 2004; Celentano *et al.*, 2005; Bueno and Villegas, 2011; Mirone *et al.*, 2019) to characterize metallic materials up to failure, remains inappropriate in this case. However, a greater fit ( $R^2=0.99$ ) is obtained by means of the following polynomial equation taking into account only necking values:

$$\sigma_{true} = -115.82\varepsilon_{true}^2 + 631.89\varepsilon_{true} + 634.59 \quad (11)$$

Both true stress-strain (obtained through Eq. (11)) and equivalent stress-true strain relationships, where equivalent stress are achieved from true stress values through Eq. (9), are shown in Fig. 8b.

Nevertheless, on ribbed bars, fitting true stress-strain data up to failure to Hollomon’s equation (Hollomon and Jaffe, 1945) results in a  $R^2$  value of 0.96 (Fig. 9). In this equation, the value of strain hardening exponent (0.1569) is lower than that obtained on fitting the same equation up to the onset of necking (0.1806). Equivalent

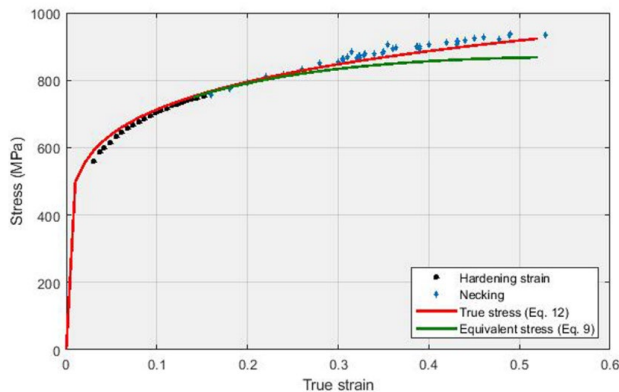


FIGURE 9. True and equivalent stress vs. true strain for ribbed bars.

stress values, according to Eq. (9) are also shown in Fig. 9.

$$\sigma_{true} = 1022.5\varepsilon_{true}^{0.1569} \quad (12)$$

A comparative analysis of the behaviour of both type of bars, leads to the conclusion regarding the influence of ribs during the necking phase, which causes an early failure. Although the onset of necking occurs earlier for round smooth bars, the

TABLE 4. Average strain and stress values at failure for smooth and ribbed bars

	$\varepsilon_{true}$	$\sigma_{true}$ (MPa)	$\sigma_{equ}$ (MPa)
Smooth	$1.028 \pm 0.027$	1175.37	969.08
Ribbed	$0.522 \pm 0.022$	923.69	867.95



Figure 10. Type of failure for smooth bars (top) and ribbed bars (bottom).

neck development range is broader, and reaches an average true strain value at failure equal to 1.028 ( $\pm 0.027$ ), while the value for ribbed bars is equal to 0.522 ( $\pm 0.022$ ). True and equivalent stress values associated to these average strain ones, obtained from Eqs. (11), (12) y (9), are shown in Table 4.

On the other hand, clear differences can be observed on the fracture shape (Fig. 10). Smooth bars show a cope & cone failure, characteristic of ductile metals. However, the failure of ribbed bars occurs on the root of one transverse rib, due to the concentration of stresses generated in this area. This phenomenon on ribbed bars has already been observed by several authors (Paul *et al.*, 2014a; Paul *et al.*, 2014b; Rocha *et al.*, 2016). A very similar failure shape is observed by Paul *et al.* (2014a), and Paul *et al.* (2014b) on high- and low-fatigue cycles. On the other hand, residual stress concentration is found by Rocha *et al.* (2016) in the same area.

#### 4. FINITE ELEMENTS ANALYSIS

The aim of this analysis involves determining the mechanical behavior of each of the two models by means of numerical methods in order to validate experimental results shown previously. In this analysis, software Ansys Workbench v16 has been used. A mechanic no-linear analysis has been introduced working, therefore, with a stress-strain relationship up to failure. In addition, bars have been modeled as an isotropic material up to yield strength, set in 500 MPa, where Young's modulus value is equal to 210 GPa and Poisson's ratio equal to 0.3. Finally, a multi-linear isotropic hardening has been used from the yield strength, based on the experimental results (Fig. 11). Regarding smooth bars, values of stress up to the onset of necking have been determined through Eq. (7). Throughout necking phase, equivalent stress values have been used, and hence Eq (9) has been applied to true stress values obtained through Eq. (11). On the other hand, Eq. (12) has been used for the behaviour of ribbed bars through-

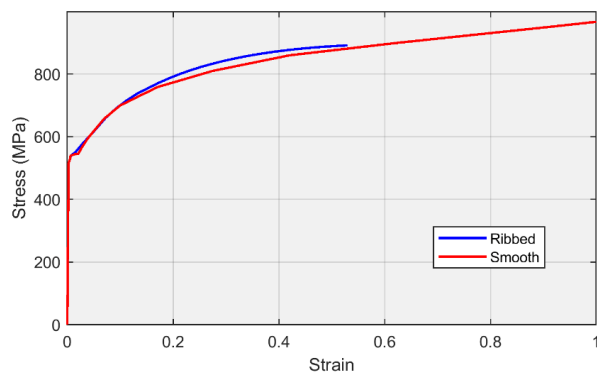


**Figure 11.** Stress-strain relationship deployed on FEM simulation for smooth (red) and ribbed (blue) models.

out the whole process. Similar to smooth bars, equivalent stress values from the onset of necking have been introduced through Eq. (9).

Due to its axial-symmetrical behaviour, a 2D analysis has been carried out for smooth round bars. The high order element Plane 183, with 8 nodes and 2 degrees of freedom at each one, was adopted. On the other hand, a higher order 3D element, Solid 186, with 20 nodes and initial hexaedrical shape, has been adopted for ribbed bars, which model has been obtained by means of 3D-scanned images of pre-test specimens. Although this shape is predominant in the core of the bar, this last element can change into a tetrahedron with 10 nodes, into a pyramid with 13 nodes or into a prism with 15 nodes, in order to adapt to the irregular ribbed geometry. Shape functions are adapted automatically when necessary. Concerning the properties of these elements, both have plasticity, stress stiffening and large strain capabilities.

On the other hand, a parametric study of tested ribbed bars has been carried out for their modeling. A higher mesh scale of critical zones, the transverse ribs and their roots have been proposed, as observed in Fig. 12.

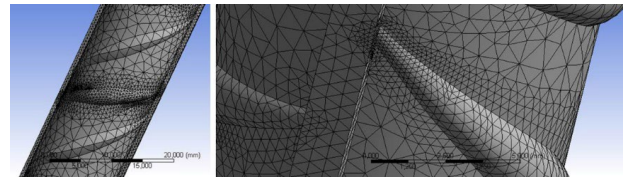


**Figure 12.** Ribbed bar mesh.

Axial displacement has been used as a control parameter during the simulation. Concerning round smooth bars, axial force has been applied upon the top of cross-section nodes, with a restricted axial displacement on the bottom cross-section ones. On the other hand, concerning ribbed bars, axial displacement has been allowed on both the top and bottom cross-section nodes, thereby applying axial

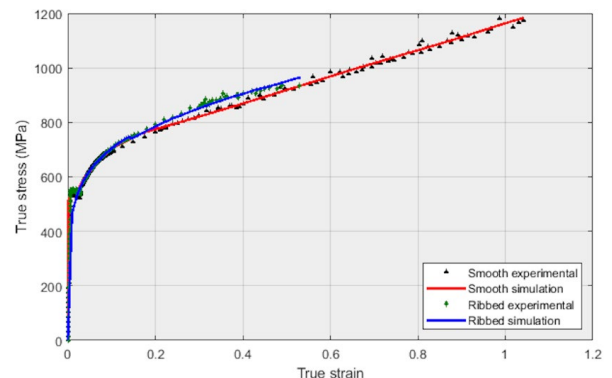


**Figure 13.** Experimental and simulation true stress-strain relationship up to failure for round smooth bars and ribbed bars (in the longitudinal axis).

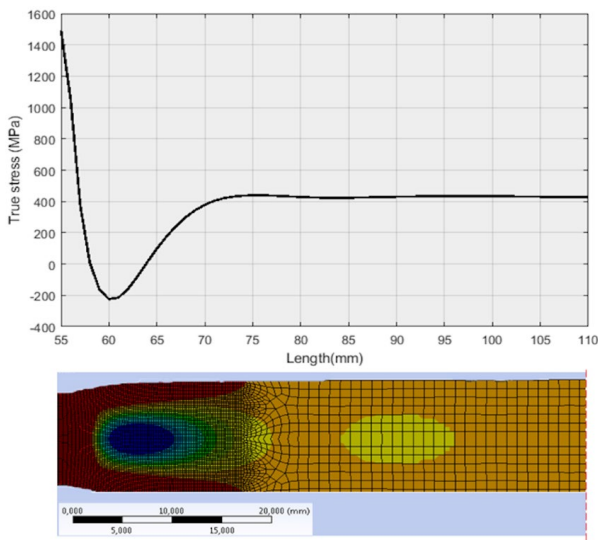


**Figure 14.** Axial stress values along the longitudinal axis on failure (top) and axial stress distribution (bottom).

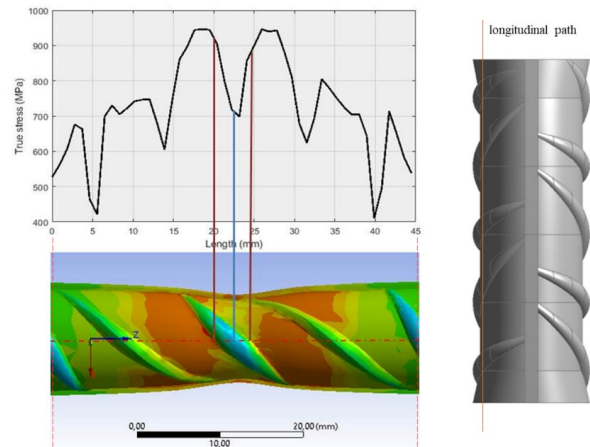


**Figure 15.** Axial stress values along a longitudinal path through the ribs on failure (up) and axial stress distribution (bottom).

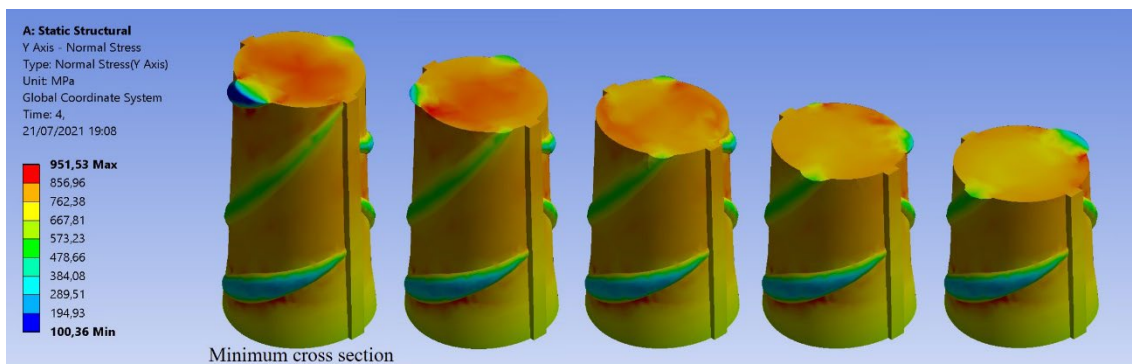


**Figure 16.** Stress distribution of several cross sections of ribbed bars affected by necking on failure.

forces upon both sections in order to guarantee the development of the minimum cross section of the neck in the half-plane bar. Furthermore, in order to block the condition of free solid and, therefore, allow the computation, a zone of 1 mm in diameter has been placed in the middle of the bar, with forbidden displacements at right angles to the longitudinal axis. Under these conditions, a very good fit between experimental and simulated stress-strain relationship is achieved for both models (Fig. 13), despite the earlier failure of ribbed one.

Regarding the stress distribution, Figs. 14 and 15 shows the results obtained for longitudinal paths in the center of smooth model and in the core boundary of ribbed one. By comparing both figures, it is evident that the existence of ribs clearly affects the behaviour of the bar through the necking. A progressive decrease in stress values can be observed in the ribbed model from the root to the middle of the transverse ribs affected by the neck, and hence, minimum values are reached at the top of this one

(Fig. 15). This stress distribution has already been proved by Rocha *et al.*, (2016) with reference to residual stresses due to manufacturing, and it suggests a large concentration of stresses at the intersection between the core and the ribs affected by necking, despite the fact of stress values are no constant along the length of this ribs. On the other hand, an irregular stress distribution is obtained in the neck cross sections (Fig. 16), reaching the higher values in the core of the bar, in a similar way to those obtained at the root of the transverse rib coincident with the minimum cross section.

It is worth to note that the differences between the experimental cross section shapes and necking profile of ribbed bars and those achieved by means of FEM simulation. Nevertheless, true stress-strain relationship up to failure is very similar in both cases, as far as the stress distribution provided by FEM model can be supposed as a reliable approximation to the mechanical behaviour of these ribbed bars throughout the necking.

## 5. CONCLUSIONS

In this research, the necking behavior of ribbed bars of Tempcore 500C carbon steel is ascertained using room-temperature tensile tests. The following conclusions can be enunciated:

- These ribbed bars behaviour is non-axial-symmetrical throughout necking phase. Therefore, based on this approach to neck symmetric geometry, those studies found in the literature with respect to the calculation of equivalent stress values on the minimum cross section of smooth bars, cannot be verified.
- A methodology based on a 3D neck analysis has been carried out in order to obtain true stress and strain values of minimum cross section throughout necking.
- Experimental results have been validated by means of Finite Elements analysis, using formulation independent of the neck geometry in order to obtain equivalent stress values.
- The results obtained for ribbed specimens have been compared to those for smooth specimens of similar steel. It has been proved that, since the ribbed geometry holds no influence on strain capacity throughout the strain hardening phase, throughout the necking this geometry considerably reduces true strain values on failure, due to the concentration of stresses placed on areas close to the root of the transverse ribs that are affected by necking.

## ACKNOWLEDGEMENTS

The authors would like to acknowledge the contribution to the experimental work carried out by J. Pinto from the School of Engineering, and G. Roldan, J.M. Jaramillo and F. Tejero from the Polytechnic School, both of University of Seville.

## REFERENCES

- Bridgman, P.W. (1944). The stress distribution at the neck of a tension specimen. *Trans. Am. Soc. Met.* 32, 553–574.
- Bueno, R., Villegas, D. (2011). Ductility in reinforcing steel: New parameter and applications. *Conference Proceedings for the 81st Annual Convention of the Wire Association International*, 46, pp. 70-76.
- Celentano, D.J., Cabezas, E.E., García, C.M., Monsalve, A.E. (2004). Characterization of the mechanical behaviour of materials in the tensile test: Experiments and simulation. *Model. Simul. Mater. Sci. Eng.* 12 (4), 425-444. <https://doi.org/10.1088/0965-0393/12/4/S09>.
- Celentano, D.J., Cabezas, E.E., García, C.M. (2005). Analysis of the Bridgman procedure to characterize the mechanical behavior of materials in the tensile test: Experiments and simulation. *J. Appl. Mech. Trans.* 72 (1), 149–152. <https://doi.org/10.1115/1.1827243>.
- Chen, J.L. (1978). *Study on metal fracture*. Metallurgical Industry Press, Beijing.
- Davidenkova, N.N., Spiridnova, N.I. (1946). Analysis of the state of stress in the neck of a tension specimen. *Proceedings—American Soc. Test. Mater.* 46, 1147–1158.
- Donato, G.H., Ganharul, G.K. (2013). Methodology for the experimental assessment for true stress-strain curves after necking employing cylindrical tensile specimens: Experiments and parameters calibration. *ASME 2013 Pressure Vessels and Piping Conference*, Vol 6A, Paris. <https://doi.org/10.1115/PVP2013-97993>.
- Dong, S., Xian, A., Mohamed, H.S., Chen, Y., Yao, J. (2019). A Simplified Analytical Solution for the Necking Semi-Empirical Stresses based on Aramis System. *KSCE J. Civ. Eng.* 23 (1), 268–279. <https://doi.org/10.1007/s12205-018-0307-0>.
- Eisenberg, M.A., Yen, C.F. (1983). An anisotropic generalization of the bridgman analysis of tensile necking. *J. Eng. Mater. Technol.* 105 (4), 264–267. <https://doi.org/10.1115/1.3225656>.
- EN 1992-1-1 (2004). *Design of concrete structures*. European Committee for Standardization, Brussels.
- EN 10080 (2005). *Steel for the reinforcement of concrete. Weldable reinforcing steel. General*. International Organization for Standardization, Geneva.
- Ganharul, G.K., De Braganza Azevedo, N., Donato, G.H. (2012). Methods for the experimental evaluation of true stress-strain curves after necking of conventional tensile specimens: Exploratory investigation and proposals. *ASME Pressure Vessels and Piping Conference* 6, 163-172. <https://doi.org/10.1115/PVP2012-78856>.
- Genovese, K., Cortese, L., Rossi, M., Amodio, D. (2016). A 360-deg Digital Image Correlation system for materials testing. *Opt. Lasers Eng.* 82, 127–134. <https://doi.org/10.1016/j.optlaseng.2016.02.015>.
- Hahn, G.T., Rosenfield, A.R. (1975). Metallurgical factors affecting fracture toughness of aluminum alloys. *Metall. Mater. Trans. A* 6, 653–668. <http://doi.org/10.1007/BF02672285>.
- Hollomon, J.H., Jaffe, L.D. (1945). Time-temperature Relations in Tempering Steel. *Trans. Am. Inst. Min. Eng.* 162, 223–249.
- Hortigón, B., Gallardo, J.M., Nieto-García, E.J., López, J.A. (2017). Elasto-plastic hardening models adjustment to ferritic, austenitic and austenoferritic Rebar. *Rev. Metal.* 53 (2), e094. <https://doi.org/10.3989/revmetalm.94>.
- Hortigón, B., Gallardo, J.M., Nieto-García, E.J., López, J.A. (2019). Strain hardening exponent and strain at maximum stress: Steel rebar case. *Constr. Build. Mater.* 196, 175–184. <https://doi.org/10.1016/j.conbuildmat.2018.11.082>.
- ISO 15630-1 (2010). *Steel for the reinforcement and prestressing of concrete. Test methods. Part 1: Reinforcing bars, wire rod and wire*. International Organization for Standardization, Geneva.
- ISO 6892-1 (2016). *Metallic materials. Tensile testing. Part 1: Method of test at room temperature*. International Organization for Standardization, Geneva.
- Kamaya, M., Kawakubo, M. (2011). A procedure for determining the true stress-strain curve a large range of strains using digital image correlation and finite element analysis. *Mech. Mater.* 43 (5), 243–253. <https://doi.org/10.1016/j.mechmat.2011.02.007>.
- La Rosa, G., Risitano, A., Mirone, G. (2003). Postnecking elastoplastic characterization: Degree of approximation in the Bridgman method and properties of the flow-stress/true-stress ratio. *Metall. Mater. Trans. A* 34 (3), 615–624. <https://doi.org/10.1007/s11661-003-0096-y>.
- Le Roy, G., Embury, J.D., Edwards, G., Ashby, M.F. (1981). A Model of Ductile Fracture Based on the Nucleation and Growth of Voids. *Acta Metall.* 29 (8), 1509–1522. [https://doi.org/10.1016/0001-6160\(81\)90185-1](https://doi.org/10.1016/0001-6160(81)90185-1).
- Li, Z., Shi, J., Tang, A. (2013). Experimental verification and analysis for Bridgman formula. *Chinese J. Appl. Mech.* 30 (4), 488–492.
- Ling, Y. (1996). Uniaxial True Stress-Strain after Necking. *AMP J. Technol.* 5, 37–48.
- Mirone, G. (2004). Approximate model of the necking behaviour and application to the void growth prediction. *Int. J. Damage Mech.* 13 (3), 241–261. <https://doi.org/10.1177/1056789504042592>.
- Mirone, G., Verleysen, P., Barbagallo, R. (2019). Tensile testing of metals: Relationship between macroscopic engineering

- data and hardening variables at the semi-local scale. *Int. J. Mech. Sci.* 150, 154–167. <https://doi.org/10.1016/j.ijmecsci.2018.09.054>.
- Nadai, A. (1950). *Theory of flow and fracture of solids*. Vol. 1, McGraw-Hill, New York.
- Norris, D.M., Moran, B., Scudder, J.K., Quiñones, D.F. (1978). A computer simulation of the tension test. *J. Mech. Phys. Solids* 26 (1), 1–19. [https://doi.org/10.1016/0022-5096\(78\)90010-8](https://doi.org/10.1016/0022-5096(78)90010-8).
- Paul, S.K., Majumdar, S., Kundu, S. (2014a). Low cycle fatigue behavior of thermo-mechanically treated rebar. *Mater. Design* 58, 402–411. <https://doi.org/10.1016/j.matdes.2014.01.079>.
- Paul, S.K., Rana, P.K., Das, D., Chandra, S., Kundu, S. (2014b). High and low cycle fatigue performance comparison between micro-alloyed and TMT rebar. *Constr. Build. Mater.* 54, 170–179. <https://doi.org/10.1016/j.conbuildmat.2013.12.061>.
- Rocha, M., Brühwiler, E., Nussbaumer, A. (2016). Geometrical and material characterization of quenched and self-tempered steel reinforcement bars. *J. Mater. Civ. Eng.* 28 (6), 04016012. [https://doi.org/10.1061/\(ASCE\)MT.1943-5533.0001355](https://doi.org/10.1061/(ASCE)MT.1943-5533.0001355)
- Rossi, M., Cortese, L., Genovese, K., Lattanzi, A., Nalli, F., Pierron, F. (2018). Evaluation of Volume Deformation from Surface DIC Measurement. *Exp. Mech.* 58 (7), 1181–1194. <https://doi.org/10.1007/s11340-018-0409-0>.
- Valiente, A. (2000). On Bridgman's Stress Solution for a Tensile Neck Applied to Axisymmetrical Blunt Notched Tension Bars. *J. Appl. Mech.* 68 (3), 412–419. <https://doi.org/10.1115/1.1360689>.
- Zhu, F., Bai, P., Zhang, J., Lei, D., He, X. (2014). Measurement of true stress-strain curves and evolution of plastic zone of low carbon steel under uniaxial tension using digital image correlation. *Opt. Lasers Eng.* 65, 81–88. <https://doi.org/10.1016/j.optlaseng.2014.06.013>.

## NOMENCLATURE

Symbol	Units	Explanation
$E$	FL <sup>-2</sup>	Young's modulus (modulus of elasticity in tension)
$F$	F	Axial force (load)
$D_0$	L	Initial cross-section diameter
$D$	L	Instantaneous cross-section diameter
$S_0$	L <sup>2</sup>	Initial cross-section area
$S$	L <sup>2</sup>	Instantaneous cross-section area
$a$	L	Radius on minimum cross-section
$r$	L	Neck curvature radius
$d_{out}$	L	Outer diameter (between longitudinal ribs)
$R$	FL <sup>-2</sup>	Engineering axial stress
$R_{p0.2}$	FL <sup>-2</sup>	Engineering yield strength computed to an offset strain of 0.2%
$R_m$	FL <sup>-2</sup>	Engineering axial strength at maximum force (also referred to as ultimate tensile strength)
$A$	dimensionless	Engineering axial strain
$A_{gt}$	dimensionless	Engineering axial strain at $R_m$
$A_t$	dimensionless	Engineering axial strain on failure
$\sigma_{true}$	FL <sup>-2</sup>	True normal stress
$\sigma_{equ}$	FL <sup>-2</sup>	Equivalent normal stress
$\epsilon_{true}$	dimensionless	True axial strain
$\epsilon_N$	dimensionless	True axial strain at the onset of necking